

# Phenomenological Model for Prediction of Cation Substitution Distribution and Some Physical Properties in $\text{Mn}^{3+}$ -Doped Barium Hexaferrite

J. Matilla-Arias<sup>1</sup> · E. Govea-Alcaide<sup>2,1</sup> · P. Mariño-Castellanos<sup>3</sup> · F. Rosales-Saiz<sup>1</sup>

Received: 25 May 2017 / Accepted: 15 June 2017 / Published online: 28 June 2017  
© Springer Science+Business Media, LLC 2017

**Abstract** The magnetic properties of M-type barium ferrite are strongly related to the distribution of  $\text{Fe}^{3+}$  cation within the crystal structure. In this work, we propose a simple phenomenological model to predict the  $\text{Fe}^{3+}$  cation distribution for  $\text{BaFe}_{12-x}\text{Mn}_x\text{O}_{19}$  compounds. From the proposed model, it was possible to estimate physical properties such as the theoretical density, the saturation magnetization, and the anisotropic constant. The obtained results were compared with experimental ones extracted from previous reported papers.

**Keywords** Barium hexaferrite · Phenomenological model · Cation distribution · Physics properties

## 1 Introduction

Doping is one of the best methods to improve general physical properties in most of the ceramic oxide materials. In particular, and due to its important technological applications,

type-M barium hexaferrite (BaM) has been doped with many elements or a combination of these ones. Some studies regarding the magnetic and microstructural properties of the BaM has been performed in relation to the substitution of Fe ions by various cations: La–Co [1], Ti–Co [2, 3], Zn–Ti [3–5], Ir–Co [2], Co–Sn [6], Mn–Ti [7], Zn–Sn [6], and Ni–Sn [6]. In addition, there are other works related to the replacement of  $\text{Fe}^{3+}$  in barium hexaferrite with only one cation such as: Ti [8, 9], Sc [10, 11], Al [12, 13] and Cr [14, 15].

The crystal structure of M-type barium hexaferrites presents a hexagonal unit cell with ten layers of O and contains a number of ions that correspond to  $2(\text{BaFe}_{12}\text{O}_{19})$  [5]. The positions of the ionic sites can be described by blocks of the type (SRS\*R\*), where R is a three-layer block ( $\text{O}_4\text{-BaO}_3\text{-O}_4$ ) with composition  $\text{BaFe}_6\text{O}_{11}$  and S is a spinel-like two-layer block ( $\text{O}_4\text{-O}_4$ ) with composition  $\text{Fe}_6\text{O}_8$ . The asterisk means the corresponding block has been turned  $180^\circ$  around the hexagonal c-axis [3]. The BaM is isostructural with magnetoplumbite ( $\text{PbFe}_{12}\text{O}_{19}$ ). In this structure, there are three types of interstitial sites that exist for Fe ions: the tetrahedral, the octahedral, and the trigonal-bipyramidal sites, respectively [3]. Thus, the smaller iron cations are distributed within five different kinds of sites: three octahedral (12k, 2a, 4f2), one tetrahedral (4f1) and one trigonal-bipyramidal site (2b) [3].

In consequence, the magnetic moment per formula unit in the BaM is the sum of the magnetic moments of the seven octahedral ions and the moment of the ion, which occupies the trigonal-bipyramidal site. This sum is reduced by magnetic moments of the ions located in both the two octahedral and the two tetrahedral sites. Theoretically, the total magnetic moment per formula unit of the BaM is  $20 \mu_B$  [16]. Therefore, any modification of the amount and the distribution of  $\text{Fe}^{3+}$  ions will change the magnetic response

✉ E. Govea-Alcaide  
egoveaalcaide@gmail.com

<sup>1</sup> Departamento de Matemática-Física, Facultad de Ciencias Informáticas, Naturales y Exactas, Universidad de Granma Apdo. 21, P. O. Box 85100, Bayamo, Cuba

<sup>2</sup> Departamento de Física, Universidade Federal do Amazonas, Manaus, Brazil

<sup>3</sup> Departamento de Química y Física, Universidad de Holguín, Holguín, Cuba

of the BaM materials, e.g., saturation magnetization, and anisotropy constant. A great number of published articles on this subject report theoretical models to predict possible modifications in the M-type ferrite with the introduction of dopants at the Fe<sup>3+</sup> sites [17, 18].

Previously, we have reported a simple phenomenological model to determine the Fe<sup>3+</sup> crystallographic site occupancy when BaM is doped with Ti<sup>4+</sup> cation [8]. In that work, we were able to calculate different parameters such as the substitution index per site, the probability of occupation per site and the amount of doping cation in each site. Also, it was possible to estimate physical properties such as the saturation magnetization [8]. The purpose of this work is to present some modifications to the phenomenological model to determine the Fe<sup>3+</sup> crystallographic site occupancy of the M-type barium hexaferrite doped with manganese. In this case, we have included the influence of the electronegativity and estimated structural and other physical properties such as the lattice energy formation, the density, the saturation magnetization, and the anisotropy constant. The selection of manganese is supported by the similitude with Fe<sup>3+</sup>. Theoretical results will be compared with previous experimental studies as reported elsewhere [17, 19–21].

## 2 Phenomenological Model

In the BaM crystal structure, there are a great number of similar crystallographic sites that can be occupied by the cationic dopants. This process can be analyzed as an interaction process between the cation and the site to be occupied. In our approximation, it is assumed that the interaction between the dopant and the site is not affected by processes occurring in other crystallographic sites. The model is only valid for low dopant concentrations per unit formula ( $x \leq 1.2$ ). Consequently, possible effects due to the distortion of the lattice are disregarded.

Considering that the doping process obeys statistical laws [8], the central parameter of the model is the Substitution Index per Site, *SIS*. This parameter can be interpreted as a measure of the site occupation probability of the dopant cation on the *i*th site and can be defined as:

$$SI_i^{Mn} = \prod_{j=1}^9 F_{i,j}^{Mn} \tag{1}$$

where  $i = 1 - 5$  is the site number, and

$$F_{i,j}^{Mn} = \begin{cases} \frac{1}{(\sqrt{2\pi}\sigma_j)} \exp\left[-\frac{\Delta m_j^2}{2\sigma_j^2}\right] & \text{if } j = 1 - 7 & (2a) \\ N_i \eta^{Mn} (1 - \eta^{Mn})^{(N_i-1)} & \text{if } j = 8 & (2b) \\ nc_i \rho^{Mn} (1 - \rho^{Mn})^{(nc_i-1)} & \text{if } j = 9 & (2c) \end{cases}$$

In (2a),  $\sigma_j = k_e m_j^{Fe}$  is the standard deviation, and  $k_e \sim 0.15$  is a value obtained according to the Pauling’s rules and the specific experimental conditions [22]. Also,  $\Delta m_j = m_j^{Mn} - m_j^{Fe}$  and  $m_j$  can be any of the following factors (see Table 1):

- 1) the cationic radius,  $R_{cat_i} = \alpha_{e_i} R_{ion}$ , where  $\alpha_{e_i}$  is a coefficient that depends on the coordination number at the *i*th site,  $nc_i$ , and  $R_{ion}$  is the ionic radius;
- 2) the electron’s valence,  $q$ ;
- 3) the atomic mass,  $m_A$ .
- 4) the ionic potential,  $P_{ion_i} = q/R_{cat_i}$ ;
- 5) the electric charge per site,  $Q_i = q/nc_i$ , where  $nc_i$  is the coordination number at the *i*th site (see Table 1);
- 6) the effective atomic number  $Z_{eff} = (Z_{cat} - q) + 2nc_i$ , where  $Z_{cat}$  is the atomic number of the cation;
- 7) and the electronegativity,  $\chi$ , (not considered in the previous work [8]).

It is important to notice that (2a) quantifies the differences between the dopant ion (Mn<sup>3+</sup>) and the host ion (Fe<sup>3+</sup>). Additionally, in (2b) and (2c) a binomial statistical distribution function was introduced to consider the relation between the occupation number of the ion in each site,  $N_i$ , and the Mn<sup>3+</sup> concentration,  $\eta^{Mn}$ , and the relation between the coordination number of the ion in each site,  $nc_i$ , and the Mn<sup>3+</sup> electronic density,  $\rho^{Mn}$ . In the same manner as in (1) and (2), it is possible to define a substitution index per site for the iron ion,  $SI_i^{Fe}$ . In this case, the “dopant” cation and the host one are the same ion, i.e.,  $\Delta m_j = 0$  [8]. Assuming that in the BaM crystal structure the conditions  $\eta^{Mn} + \eta^{Fe} = 1$  and  $\rho^{Mn} + \rho^{Fe} = 1$  is fulfilled, then (2) yields:

$$F_{i,j}^{Fe} = \begin{cases} 1/(\sqrt{2\pi}\sigma_j) & \text{for } j = 1 - 7 & (3a) \\ N_i \eta^{Fe} (1 - \eta^{Fe})^{(N_i-1)} & \text{if } j = 8 & (3b) \\ nc_i \rho^{Fe} (1 - \rho^{Fe})^{(nc_i-1)} & \text{if } j = 9 & (3c) \end{cases}$$

where  $\eta^{Fe}$  is the Fe<sup>3+</sup> concentration per site.

Taking into account all the above ideas, we were able to define the occupation probability of Fe<sup>3+</sup> and Mn<sup>3+</sup> ions, respectively, as:

$$S_i = \begin{cases} \left( \frac{SI_i^{Fe}}{SI_i^{Mn} + SI_i^{Fe}} \right) \frac{N_i}{Nt} & \text{for Fe}^{3+} \text{ ion} & (4a) \\ \left( \frac{SI_i^{Mn}}{SI_i^{Mn} + SI_i^{Fe}} \right) \frac{N_i}{Nt} & \text{for Mn}^{3+} \text{ ion} & (4b) \end{cases}$$

where  $Nt = \sum_{i=1}^5 N_i = 12$  is the total site number of Fe<sup>3+</sup> cations per unit formula in the BaM structure. It is important to take into account that the occupation probability of the Fe<sup>3+</sup>,  $SI_i^{Fe}$ , can be interpreted as analogous to the relative areas in each site of the Mössbauer spectrum

**Table 1** Values of the factors in calculations: the atomic number,  $Z_{cat}$ , the electron’s valence,  $q$ , the ionic ratio,  $R_{ion}$ , the atomic mass,  $m_A$ , and the electronegativity,  $\chi$

Ion	$Z_{cat}$	$q$	$R_{ion}$	$m_A$	$\chi$
Fe <sup>3+</sup>	26	3	0.64	55.85	1.8
Ba <sup>2+</sup>	56	2	1.34	137.36	0.9
O <sup>2-</sup>	8	2-	1.40	16.00	3.5
Mn <sup>3+</sup>	25	3	0.67	54.94	1.5
Site	2a	2b	4f1	4f2	12k
$nc_i$	6	5	4	6	6
$N_i$	1	1	2	2	6

We have also included values of the coordination number,  $nc$ , and the occupation number for each iron site. See text for details

[19]. Under this condition, it is possible to define the site occupation number of Fe<sup>3+</sup> and Mn<sup>3+</sup> ions as [19]:

$$Q_i^{Fe} = (Nt - x) \frac{S_i^{Fe}}{\sum_{i=1}^5 S_i^{Fe}}, \tag{2}$$

and

$$Q_i^{Mn} = N_i - Q_i^{Fe}. \tag{3}$$

We want to remark that the essence of the model is that the doping process obeys statistical laws. In line with that statement, we have used two distinct probabilistic statistical functions to describe: (i) the difference between the dopant and the host ions (see (2b)) and (ii) the interaction between the dopant ion and the site (see (2b) and (2c)). In addition, all the input data for calculations were listed in Table 1. In the next section, we present some physical parameters can be expressed within the framework of the phenomenological model presented above.

### 2.1 Lattice Formation and Physical Properties Calculations

The reticular energy,  $U_{POT}$ , is an important parameter to establish the existence and stability of ionic solids structure [23]. In most of the cases, its direct determination is not possible. Glasser et al. proposed a generalization of the Kapustinskii equation’s in order to calculate  $U_{POT}$  in ionic compounds with multiple ions [24]. Under the framework of the model presented in the above section, the generalized Kapustinskii equation for the total reticular energy adopts the form:

$$U_{POT} = U_{Ba} + \sum_{i=1}^5 U_i + U_O, \tag{4}$$

here  $U_{Ba}$  is the contribution barium atom given by:

$$U_{Ba} = \frac{A}{\langle r \rangle} \left( 1 - \frac{\sigma}{\langle r \rangle} \right) q_{Ba}^2, \tag{5}$$

$U_i$  is the contribution of both the host and the dopant cation at the  $i$ th-site expressed as:

$$U_i = \frac{A}{\langle r \rangle} \left( 1 - \frac{\sigma}{\langle r \rangle} \right) (q_{Fe}^2 Q_i^{Fe} + q_{Mn}^2 Q_i^{Mn}), \tag{6}$$

and  $U_O$  is the contribution of the oxygen atoms to the total reticular energy that is given by:

$$U_O = \frac{A}{\langle r \rangle} \left( 1 - \frac{\sigma}{\langle r \rangle} \right) 19q_O^2. \tag{7}$$

In (5)–(7),  $A = 1213.9 \text{ kJmol}^{-1} \text{ \AA}$ ,  $\langle r \rangle$  is the weighted-mean cation-anion distance,  $\sigma$  is a compressibility constant describing the repulsions between the ions (usually chosen  $\sigma = 0.345 \text{ \AA}$ ) [24] and  $q_{Fe}$ ,  $q_{Mn}$ ,  $q_{Ba}$  and  $q_O$  are the valence of Fe<sup>3+</sup>, Mn<sup>3+</sup>, Ba<sup>2+</sup>, and O<sup>2-</sup> ions, respectively (see Table 1).

By using (4) for the total reticular energy, then the theoretical density of materials adopts the form [24]:

$$\rho_{mod} = \frac{10^{24} M_m}{N_A 2I^4} \left( \frac{U_{POT}}{A} \right)^3 \tag{8}$$

where the factor  $10^{24}$  converts  $\text{\AA}^3$  to  $\text{cm}^3$ ,  $N_A$  is the Avogadro’s number,  $M_m$  is the molecular mass of the compound, and

$$I = \frac{1}{2} \left( q_{Fe}^2 \sum_{i=1}^5 Q_i^{Fe} + q_{Mn}^2 \sum_{i=1}^5 Q_i^{Mn} + q_{Ba}^2 + 19q_O^2 \right) \tag{9}$$

is the ionic strength parameter.

The theoretical saturation magnetization can be obtained from the previous model assuming a collinear array of magnetic moments of cations in the BaM [8] as:

$$M_s = \sum_{i=1}^5 \left( \mu^{Fe} Q_i^{Fe} + \mu^{Mn} Q_i^{Mn} \right), \tag{10}$$

where  $\mu^{Fe}$  and  $\mu^{Mn}$  are the magnetic moments, at  $T = 0 \text{ K}$ , of Fe<sup>3+</sup> and Mn<sup>3+</sup> cations, respectively, taken from Table 6.1 of Chapter 6, Reference [25]. Also, the theoretical anisotropy constant can be described as:

$$K_1 = \sum_{i=1}^5 k_i Q_i^{Fe}, \tag{11}$$

here,  $k_i$  is the value of the anisotropy constant for Fe<sup>3+</sup> cations at the  $i$ th-site, taken from Reference [26].

### 3 Results and Discussion

For a better understanding of our results, it is important to remark that the presented model can be used only in the case of one dopant cation and for dopant concentrations less than  $x = 1.2$ . Also, the obtained results correspond to ideal substitutions and are not related to any synthesis method. The theoretical results will be compared to experimental data obtained under two different preparation methods. On the one hand, Lee et al. have synthesized powders of Mn<sup>3+</sup>-substituted M-type Ba-ferrite BaFe<sub>12-x</sub>Mn<sub>x</sub>O<sub>19</sub> with  $x = 0, 2, 4, 6$ ) by using the high temperature thermal decomposition method [19]. On the other hand, Sharma et al. have reported the use of the high-energy ball milling method to prepare Mn<sup>3+</sup>-substituted Ba-ferrite BaFe<sub>12-x</sub>Mn<sub>x</sub>O<sub>19</sub> with 0.1, 0.2, 0.3, 0.4, and 0.5 [20] and  $x = 0.5, 1.0, 1.5, 2.0$  [21]. In those works, the Fe<sup>3+</sup> site occupation distribution studies were performed by using the Mössbauer spectroscopy.

Figure 1 shows the theoretical and the experimental values of the site occupation number of Fe<sup>3+</sup> ion, for BaFe<sub>12-x</sub>Mn<sub>x</sub>O<sub>19</sub> with  $x = 0, 0.5, 1.0, 1.5, 2.0$ . Notice that the theoretical and the experimental values of  $Q_i^{\text{Fe}}$  exhibit similar qualitative behavior, i.e.,  $Q_i^{\text{Fe}}$  decreases with increasing the Mn<sup>3+</sup> content in all sites. This suggests that Mn<sup>3+</sup> can substitute the Fe<sup>3+</sup> ion in all sites mostly due to the similitude between both ions (see Table 1). However, the above statement is more marked in the site 12k (5.712) in good agreement with that reported in Refs. [19, 20]. I was found that the theoretical and the experimental values of  $Q_i^{\text{Fe}}$  show appreciable quantitative differences for  $x \geq 1.0$ . That is not an unexpected result considering that the model is for low dopant concentrations, as mentioned above.

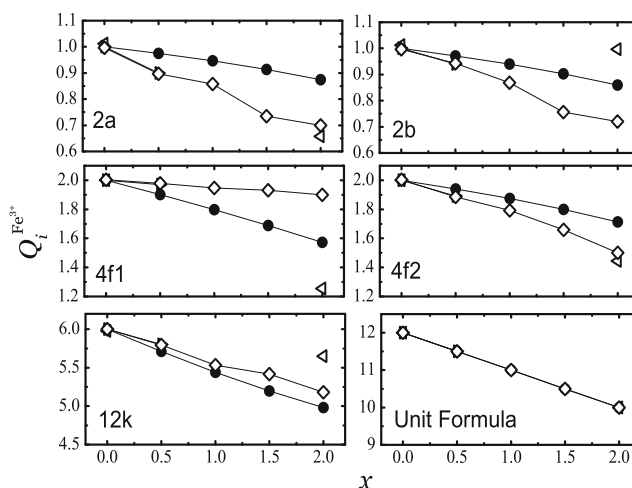


**Fig. 1** Theoretical and experimental values of the site occupation number of the Fe<sup>3+</sup> ion ( $Q_i^{\text{Fe}}$ ), for BaFe<sub>12-x</sub>Mn<sub>x</sub>O<sub>19</sub> with  $x = 0, 0.5, 1.0, 1.5, 2.0$ . The lines between the points are guide for the eyes. Symbology: – ● – Model Calculation, – ◁ – Reference [19], – ▷ – Reference [20], – ◊ – Reference [21]

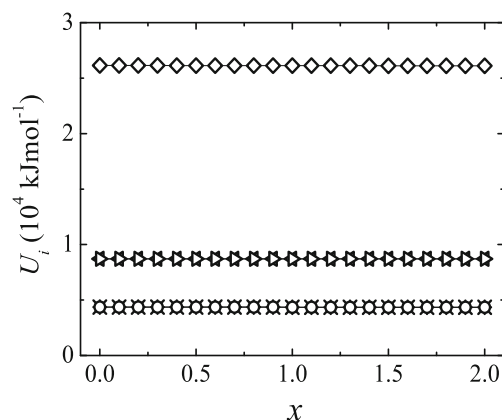


**Fig. 2** Contribution of cation and dopant to the total reticular energy at the  $i$ th-site ( $U_i$ ) as function of dopant concentration per unit formula ( $x$ ) in BaFe<sub>12-x</sub>Mn<sub>x</sub>O<sub>19</sub>. Symbology for sites: – \* – 2a, – ◦ – 2b, – ◁ – 4f1, – ▷ – 4f2, – ◊ – 12k

Taking into account values of  $Q_i^{\text{Fe}}$ , Fig 2 displays the generated values of the total reticular energy for different values of dopant concentration. In this case, the results indicate that the influence of the Mn<sup>3+</sup> content on the  $U_i$  is negligible. According to (6), the reticular energy depends on  $Q_i^{\text{Fe}}$  and  $Q_i^{\text{Mn}}$ . However, as the electron valence and the ionic ration of Fe<sup>3+</sup> and Mn<sup>3+</sup> are almost the same, then, substituting (2) and (3) into (6) yields that  $U_i \propto N_i$ .

Table 2 displays the theoretical values of volume density,  $\rho_{\text{mod}}$ , for the BaFe<sub>12-x</sub>Mn<sub>x</sub>O<sub>19</sub> ( $x = 0, 2, 4$ , and 6). The experimental density values,  $\rho_{\text{exp}}$ , extracted from Ref. [19] were also reported. In all cases,  $\rho_{\text{mod}}$  is less than  $\rho_{\text{exp}}$  obtained by using the Rietveld refinement method [19]. However, the discrepancy between both values do not exceed

**Table 2** Total reticular energy,  $U_{POT}$ , of the  $BaFe_{12-x}Mn_xO_{19}$  compound calculated by using (4)

$x$	$U_{POT}$ ( $\times 10^4 kJmol^{-1}$ )	$\rho_{mod}$ ( $g/cm^3$ )	$\rho_{exp}$ ( $g/cm^3$ )	$(\rho_{mod} - \rho_{exp})/\rho_{exp}$ (%)
0	9.10	4.982	5.285	5.7
2	9.09	4.956	5.278	6.1
4	9.08	4.930	5.267	6.4
6	9.07	4.905	5.257	6.7

Values of the theoretical density,  $\rho_{mod}$ , and the experimental density,  $\rho_{exp}$ , are presented. Values of  $\rho_{exp}$  were extracted from Ref. [19]

7% being considered as a good approximation. It is important to notice that both densities are nearly dopant independent because of similarities between  $Fe^{3+}$  and  $Mn^{3+}$  ions. Moreover, the obtained values for the theoretical density give credence to our assumptions to determine the reticular energy for the BaM.

Figure 3a displays the influence of the  $Mn^{3+}$  content on the experimental and the generated curves of saturation magnetization of  $BaFe_{12-x}Mn_xO_{19}$ , with  $x$  in the range 0 to 2.0. Experimental values of  $M_s$ , were extracted from Refs. [19–21]. It was found that the qualitative behavior of both curves are similar, i.e.,  $M_s$  decreases with increasing the dopant content. The above behavior is more evident in the experimental curve and can be explained considering that the  $Mn^{3+}$  ion tends to occupy the spin up sites (12k, 4f2 and 2a) as observed in Fig. 1. Also, it is possible notice that, at 0 K, the magnetic moment of the  $Mn^{3+}$  ion ( $4.0\mu_B$ ) is less than the  $Fe^{3+}$  ion ( $5.0\mu_B$ ). Thus, the higher the Mn content is, the lower the  $M_s$ . Additionally, Fig. 3a shows quantitative

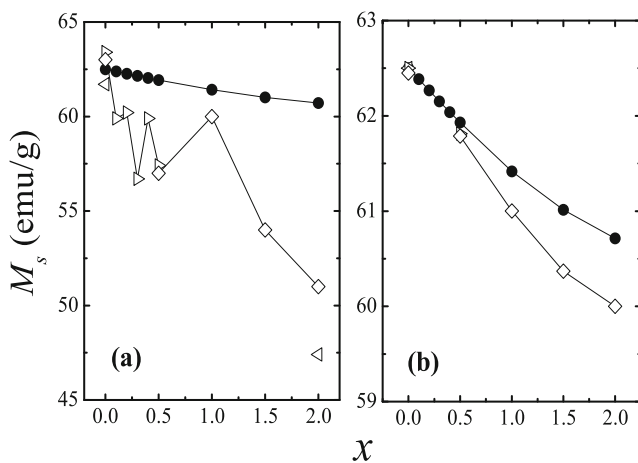


**Fig. 3** Theoretical and experimental values of saturation magnetization ( $M_s$ ), for the  $BaFe_{12-x}Mn_xO_{19}$  system. The lines between the points are guide for the eyes. Symbology: —●— Model Calculation, —◁— Reference [19], —▷— Reference [20], —◇— Reference [21]

differences between the theoretical and experimental values of saturation magnetization. In real samples, such differences indicate that the assumption of the collinear array of magnetic moments in the unit cell is no longer valid.

We have also calculated  $M_s$  by using (10) and the experimental values of  $Q_i^{Fe}$  from the Mössbauer spectroscopy reported in the Ref. [19–21] and presented in Fig. 1; the obtained results are shown in Fig. 3b. In this case, theoretical and experimental curves exhibit very similar behavior given credence to the previous analysis. It is possible to notice that even for  $x = 2.0$ , the theoretical value of  $M_s$  is only 1% higher than the experimental one.

Additionally, we have estimated the theoretical anisotropy constant,  $K_1^{mod}$  of  $BaFe_{12-x}Mn_xO_{19}$  and the results for different values of  $x$  are shown in Table 3. In the later, were also included experimental values of the anisotropy constant,  $K_1$ , extracted from Refs. [17] and [19]. As inferred from the results, the substitution of the  $Fe^{3+}$  by the  $Mn^{3+}$  ion provokes a decrease in the anisotropy constant with increasing dopant concentration. From previous analysis, it is reasonable to assume that the above behavior is related to the preferential occupation of the site 12k by the dopant cation. Also, appreciable quantitative differences between experimental and theoretical values were found, a fact mostly related to the assumption of the single ion model to calculate the anisotropy constant. Notice that for  $BaFe_{12}O_{19}$ , the anisotropy constant obtained by using the single ion model is  $1.93 cm^{-1}/molecule$  and experimentally this value is  $8.08 cm^{-1}/molecule$  [26].

Finally, we want to point out that the proposed model assumes ideal substitutions of the dopant cation at  $Fe^{3+}$  sites. Recently, Nemrava et al. [27] have reported the existence of three oxidation states of manganese in the barium hexaferrite, i.e.,  $Mn^{2+}$ ,  $Mn^{3+}$ , and  $Mn^{4+}$ . According to that study, the  $Mn^{2+}$  occupies the tetrahedral site, while  $Mn^{3+}$  and  $Mn^{4+}$  the octahedral site. Such complex physical scenario can explain the differences between the theoretical findings and the experimental results reported in Fig. 1. It is possible to notice that in the proposed model we have considered one oxidation state for manganese, i.e.,  $Mn^{3+}$ .

**Table 3** Values of anisotropy constant for the pure and the doped BaM compound

$x$	$K_1^{mod}$ ( $\times 10^6 erg/cm^3$ )	$K_1$ ( $\times 10^6 erg/cm^3$ )	Reference
0	0.79	2.90	[19]
1.5	0.72	2.70	[17]
2.0	0.69	2.20	[19]

Here,  $K_1^{mod}$  is the theoretical anisotropy constant and  $K_1$  is the experimental anisotropy constant

## 4 Conclusions

A simple phenomenological model based on statistical considerations was presented. From the obtained results, it was possible to estimate the  $\text{Fe}^{3+}$  cation distribution of the  $\text{BaFe}_{12-x}\text{Mn}_x\text{O}_{19}$  compound for different values of  $x$ . Values of the site occupation number indicated that the preferential site for the dopant ion ( $\text{Mn}^{3+}$ ) is the 12k. In all cases, the proposed model and the experimental values exhibited similar qualitative and quantitative behavior for  $x \leq 1.2$ . Based on the performed analysis, it is possible to assure that the phenomenological model is a simple and useful tool for the prediction of cation substitution distribution in M-type barium hexaferrites.

## References

- Pieper, M.W., Morel, A., Kools, F.: NMR analysis of La+Co doped M-type ferrites. *J. Magn. Magn. Mater.* **242–245**, 1408–1410 (2002)
- Kreisel, J., Vincent, H., Tasset, F., Paté, M., Wolfers, P.: A single-crystal neutron diffraction study of the magnetic anisotropy change in Ba-hexaferrites. *Physica B.* **276–278**, 688–689 (2000)
- Rösler, S., Waterwig, P., Langbein, H.: Synthesis and characterization of hexagonal ferrites  $\text{BaFe}_{12-2x}\text{Zn}_x\text{Ti}_x\text{O}_{19}$  ( $0 \leq x \leq 2$ ) by thermal decomposition of freeze-dried precursors. *Cryst. Res. Technol.* **38**, 927–934 (2003)
- Haijun, Z., Zhichao, L., Chengliang, M., Xi, Y., Liangying, Z., Mingzhong, W.: Complex permittivity, permeability, and microwave absorption of Zn- and Ti-substituted barium ferrite by citrate sol-gel process. *Mat. Sci. Eng. B* **96**, 289–295 (2002)
- Wartewig, P., Krause, M.K., Esquinazi, P., Rösler, S., Sonntag, R.: Magnetic properties of Zn- and Ti-substituted barium hexaferrite. *J. Magn. Magn. Mater.* **192**, 83–99 (1999)
- Lisjak, D., Drogenik, M.: Synthesis and characterization of ASn-substituted ( $A=\text{Zn}, \text{Ni}, \text{Co}$ ) BaMhexaferrite powders and ceramics. *J. Eur. Ceram. Soc.* **24**, 1841–1845 (2004)
- Bashkurov, S.S., Liberman, A.B., Valiullin, A.A., Zaripova, L.D., Kokin, S.V.: Effect of  $\text{Mn}^{2+}$  ions on the magnetic microstructure of hexaferrites. *Phys. Solid State* **42**, 79–83 (2000)
- Mariño, P.A., Moreno, A.C., Orozco, G., Garcia, J.A., Govea, E.: Structural and magnetic study of the  $\text{Ti}^{4+}$ -doped barium hexaferrite ceramic samples: Theoretical and experimental results. *Physica B.* **406**, 3130–3136 (2011)
- Mariño-Castellanos, P.A., Anglada-Rivera, J., Cruz-Fuentes, A., Lora-Serrano, R.: Magnetic and microstructural properties of the  $\text{Ti}^{4+}$ -doped Barium hexaferrite. *J. Magn. Magn. Mater.* **280**, 214 (2004)
- Chesnokov, A.G., Naiden, E.P.: Influence of diamagnetic cations  $\text{Sc}^{3+}$  on the magnetoelastic energy of M-type hexaferrites. *Phys. Solid State* **43**, 1728–1730 (2001)
- Kamzin, A.S.: Surface magnetism of Sc-substituted Ba-M hexaferrites. *JETP* **89**, 890–898 (1999)
- Popov, M.A., Zavislyak, I.V., Tatarenko, A.S., Srinivasan, G., Balbashov, A.M.: Magnetic and dielectric excitations in the W-Band in aluminum substituted barium and strontium hexaferrites. *IEEE Trans. Magn.* **45**, 2053–2058 (2009)
- Choi, D.H., An, S.Y., Lee, S.W., Shim, I., Kim, C.h.S.: Site occupancy and anisotropy distribution of Al substituted Ba-ferrite with high coercivity. *Phys. Stat Sol. B* **241**, 1736–1739 (2004)
- Ounnunkad, S., Winotai, P.: Properties of Cr-substituted M-type barium ferrites prepared by nitrate/citrate gel-autocombustion process. *J. Magn. Magn. Mater.* **301**, 292–300 (2006)
- Kim, Ch.S., An, S.Y., Son, J.H., Lee, J., Oak, H.N.: Magnetic properties of  $\text{Cr}^{3+}$  substituted  $\text{BaFe}_{12}\text{O}_{19}$  powders grown by a sol-gel method. *IEEE Trans. Magn.* **35**, 3160–3162 (1999)
- Parker, J., Studders, R.J. (eds.): *Permanent Magnets and Their Application*, vol. 406. Wiley, New York (1962)
- Geiler, A.L., Yang, A., Zuo, X., Yoon, S.D., Chen, Y., Harris, V.G., Vittoria, C.: Atomic scale design and control of cation distribution in hexagonal ferrites. *Phys. Rev. Lett.* **101**, 067201 (2008)
- Wu, C., Yu, Z., Yang, Y., Sun, K., Nie, J., Liu, Y., Jiang, X., Lan, Z.: Computational and experimental study on the cation distribution of La-Cu substituted barium hexaferrites. *J. Alloys Compd* **664**, 406–410 (2016)
- Lee, I.K., Sur, J.C., Shim, I.B., Kim, C.S.: The effect of manganese substituted M-type hexagonal Ba-ferrite. *J. Magn.* **14**(2), 93–96 (2009)
- Sharma, P., Rocha, R.A., Medeiros, S.N., Hallouche, B., Paesano, Jr. A.: Structural and magnetic studies on mechano-synthesized  $\text{BaFe}_{12-x}\text{Mn}_x\text{O}_{19}$ . *J. Magn. Magn. Mater.* **316**, 2933 (2007)
- Sharma, P., Rocha, R.A., De Medeiros, S.N., Paesano, Jr. A., Hallouche, B.: Structural, Mössbauer and magnetic studies on Mn-substituted barium hexaferrites prepared by high energy ball milling. *Hyperfine Interact.* **175**, 77–84 (2007)
- Chiang, Y.M., Birnie, D.P., Kingery, W.D. (eds.): *Physical Ceramics*, vol. 522. Wiley, New York (1997)
- Glasser, L.: Lattice energies of crystals with multiple ions: a generalized Kapustinskii equation. *Inorg. Chem.* **34**(20), 4935–4936 (1995)
- Glasser, L., Brooke Jenkins, H.D.: Lattice energies and unit cell volumes of complex ionic solids. *J. Amer. Chem. Soc.* **122**(4), 632–638 (2000)
- Cullity, B.D., Graham, C.D.: *Introduction to Magnetic Materials*, vol. 177. Wiley, New Jersey (2009)
- Xu, Y., Yang, G.L., Chu, D.P., Zhai, H.R.: Magnetic anisotropy of BaM ferrites. *J. Magn. Magn. Mater.* **31–34**, 815–816 (1983)
- Nemrava, S., Vinnik, D.A., Hu, Z., Valldor, M., Chang-Yang, K., Zherebtsov, D.A., Gudkova, S.A., Chien-Te, C., Hao Tjeng, L., Niewa, R.: Three oxidation states of manganese in the barium hexaferrite  $\text{BaFe}_{12-x}\text{Mn}_x\text{O}_{19}$ . *Inorg. Chem.* **56**, 3861–3866 (2017)